Eye (2016) 30, 901–916

www.nature.com/eye

REVIEW

Advances of optical coherence tomography in myopia and pathologic myopia

DSC Ng, CYL Cheung, FO Luk, S Mohamed, ME Brelen, JCS Yam, CW Tsang and TYY Lai

Abstract

The natural course of high-axial myopia is variable and the development of pathologic myopia is not fully understood. Advancements in optical coherence tomography (OCT) technology have revealed peculiar intraocular structures in highly myopic eyes and unprecedented pathologies that cause visual impairment. New OCT findings include posterior precortical vitreous pocket and precursor stages of posterior vitreous detachment; peripapillary intrachoroidal cavitation; morphological patterns of scleral inner curvature and dome-shaped macula. Swept source OCT is capable of imaging deeper layers in the posterior pole for investigation of optic nerve pits, stretched and thinned lamina cribrosa, elongated dural attachment at posterior scleral canal, and enlargement of retrobulbar subarachnoid spaces. This has therefore enabled further evaluation of various visual field defects in high myopia and the pathogenesis of glaucomatous optic neuropathy. OCT has many potential clinical uses in managing visual impairing conditions in pathologic myopia. Understanding how retinal nerve fibers are redistributed in axial elongation will allow the development of auto-segmentation software for diagnosis and monitoring progression of glaucoma. OCT is indispensable in the diagnosis of various conditions associated with myopic traction maculopathy and monitoring of post-surgical outcomes. In addition, OCT is commonly used in the multimodal imaging assessment of myopic choroidal neovascularization. Biometry and topography of the retinal layers and choroid will soon be validated for the classification of myopic maculopathy for utilization in epidemiological studies as well as clinical trials.
Eye (2016) **30,** 901–916; doi:10.1038/eye.2016.47; published online 8 April 2016

Introduction

Myopia is a major growing public health problem worldwide. Pathologic myopia is defined as myopia with complications of the posterior segment associated with progressive and excessive elongation of the globe. It is accompanied by various degenerative changes in the posterior segment structures including the sclera, optic disc, choroid, Bruch's membrane, retinal pigment epithelium (RPE), and neural retina. Pathologic myopia has been found to be one of the leading causes of visual impairment in many developed countries.[1] Asian populations are well known for having the highest rates of myopia in the world with increasing prevalence and severity rates from population-based studies.[2] The cut-off value of high-axial myopia varied (between refractive error of − 6 to − 8 diopters (D) or axial length of 26–26.5 mm) among population-based or histological studies and beyond these values, the prevalence of pathologic myopia increases exponentially.[3]

Optical coherence tomography (OCT) has been widely used for assessing retina and optic nerve by providing quantitative and qualitative assessment of macula and retinal nerve fiber layer (RNFL) in the last decade. Before the use of OCT, the pathological changes of highly myopic eyes in human could only be studied in enucleated globes and ocular structures were measured histomorphometrically. Jonas *et al* recently reviewed the histological changes of high-axial myopia.[4] In brief, there is profound thinning of the choroid associated with the loss of choriocapillaris and RPE. The thinning of the sclera starts at or behind the equator with maximal thinning at the posterior pole, and the elongated peripapillary scleral flange (defined as the canal between the optic nerve border and the point where dura mater merges with the sclera) and lamina cribrosa is stretched thin with subsequent decreased distance between the

Department of Ophthalmology & Visual Sciences, The Chinese University of Hong Kong, Hong Kong Eye Hospital, Hong Kong, China

Correspondence:
DSC Ng, Department of Ophthalmology & Visual Sciences, The Chinese University of Hong Kong, Hong Kong Eye Hospital, 147K Argyle Street, Hong Kong, China
Tel: +852 29465858;
Fax: +852 27159490.
E-mail: dannyng@cuhk.edu.hk

Received: 12 October 2015
Accepted in revised form: 29 January 2016
Published online: 8 April 2016

retrobulbar cerebrospinal fluid space with the intraocular pressure compartment. The weakened peripapillary scleral flange may have a consequence for the biomechanical stability of the lamina cribosa and the nerve fibers passing through it. Although histological studies have provided valuable information regarding the structure of highly myopic eyes, the examinations were performed after postmortem or after enucleation. Therefore, these results might have been influenced by deformation during fixation and sectioning. With the advent of OCT, *in vivo* studies of the structure of highly myopic eyes became possible.

The natural course of high myopia is variable, while some eyes maintain vision with relatively minor changes; others developed pathologic myopia due to a spectrum of visual threatening conditions.[5] OCT has revealed peculiar minute and subtle intraocular deformities in highly myopic eyes, which has not been clearly observed in histological studies or with other *in vivo* imaging modalities such as ultrasonography or magnetic resonance imaging (MRI).[6] It allows the analysis of spatial relationship between various layers at the posterior pole. OCT studies of altered biometry and topography of retinal and choroidal layers enabled evaluation of their correlations with demographics, visual function, and fundoscopic observations in pathologic myopia.[7] Furthermore, OCT is indispensable in the diagnosis and monitoring of the spectrum of visual impairing conditions, for example, glaucoma and diabetic macular edema. This review summarizes current findings on the application of OCT as a tool to study pathologic myopia and discuss the clinical implications of these findings as well as future research directions.

Principles of OCT

Because light travels in high speed (3×10^8 m/s), it is impossible to measure the time-of-flight delay within the eyeball with any external measurement system. However, it is possible to time how long light takes to travel a given distance using its wave-like character. Coherency of light is a measure of how one wave of light is correlated with another and coherence length is the distance light would need to travel during the coherence time. Images with micron-scale level of resolution could be achieved by comparing the time of flight of the sample reflection with the known delay of a reference reflection by using interference to find phase differences in light waves.[8] This is the basis for time-domain (TD) OCT, in which a small portion of tissue is sampled at a single time point. TD OCT is not efficient because longer duration of time is needed to acquire the image of the entire posterior pole.

Spectral domain (SD) OCT is the second generation of OCT that takes light from the interferometer and passes in through a grating to separate out the component wavelengths. Using a Fourier transform it is possible to determine where, and how strongly, different reflections in the sample arm originated from, simultaneously. SD OCT is, therefore, much more efficient (up to 100 times faster than TD OCT) in extracting image of all tissue layers at any given light exposure.

When the peak sensitivity of SD OCT is placed posteriorly at the inner sclera, deeper structures such as the choroid can be seen. Enhanced depth imaging (EDI) with SD OCT, by positioning the choroid–scleral interface adjacent to the zero delay, can now provide a non-invasive way to increased visualization of the choroidal anatomy.[9] It can be performed in commercialized SD OCT instruments by selecting the EDI function in the software.

Swept source (SS) OCT is the latest generation of OCT that uses a laser that sweeps across a range of wavelengths in an orderly fashion. The interference of the light from the sample and reference arms produces a signal that can be read out in nearly real-time by a photodiode.[10] This light source is inherently more complicated than what is used by SD OCT and the detectors in SS OCT are capable of operating at higher speeds. Lasers used in SS OCT have longer wavelength, which has improved ability to penetrate through tissue to a greater extent, in particular tissue that contains melanin.[11] SS OCT have enabled high-resolution images of the vitreous and vitreo–retinal interface; fine delineation of the choroid layer; better visibility of the entire thickness of the sclera, lamina cribrosa, and the retrobulbar subarachnoid space.[11]

Assessment of vitreous by OCT in myopia

Kishi used fluorescein stain in autopsy eyes to demonstrate that the liquefied lacuna anterior to the macular area was physiologically found to be present in adults and named it the posterior precortical vitreous pocket (PPVP).[12] The posterior wall of PPVP consists of a thin layer of vitreous cortex and its anterior wall is vitreous gel. Further studies demonstrated the presence of PPVPs during triamcinolone-assisted vitrectomy.[13] The *in vivo* structure and physiological function of PPVP have eluded scientists and vitreoretinal surgeons in the past using biomicroscopy and B-scan ultrasonography. TD OCT could only depict the vitreous cortex when it was slightly detached from the retina but failed to show the inner structure of the vitreous. SD OCT allowed the first visualization of PPVP *in vivo* but has low sensitivity with limited scan length despite EDI OCT.[14] With increased scan length of 12mm and improved resolution,

visualization of the vitreoretinal interface is enhanced by using SS OCT (Figure 1). Itakura *et al*[15] was able to observe the boat-shaped configuration of PPVP and the connecting channel within PPVP, which suggested that it may not be an isolated lacunae with possible route to the aqueous humor. However, even with extended imaging protocols and en face imaging, SS OCT was still unable to detect the entire superior border of the PPVP in vast majority of subjects and the communication between PPVP with the anterior chamber is not yet fully understood.[16–18]

SS OCT demonstrated that the size of PPVP increases with increasing severity of myopia.[15] Larger PPVP reflects earlier vitreous liquefaction in high myopia, which may predispose partial and subsequently complete posterior vitreous detachment (PVD). With SS OCT, the precursor stages of PVD in high-myopia subjects were observed for the first time *in vivo*. Before the development of a complete PVD with a Weiss ring, PVD began in the paramacular area and progressed to a perifoveal PVD and later vitreomacular separation (Figure 1a). This finding correlates well with the clinical observation that PVD occurs in younger age in highly myopic eyes compared with non-myopic eyes.[19]

Residual vitreous cortex has been noted by surgeons in patients treated for vitreomacular diseases despite the apparent PVD with a Weiss ring and was called 'vitreoschisis'[20] (Figure 1b). It was observed that vitreous cortex frequently remained on the retina in highly myopic eyes despite a Weiss ring. Using SS OCT in a case–control study, Itakura *et al*[21] found the presence of residual vitreous cortex in 40.5% of highly myopic eyes, compared with only 8.7% of controls. Vitreoschisis may be related to the underlying multi-lamellar structure of the posterior wall of PPVP, which can be split into separate layers during anomalous PVD. The peculiar structure of PPVP has a key role in various vitreomacular disorders and contradicts with the conventional concept that

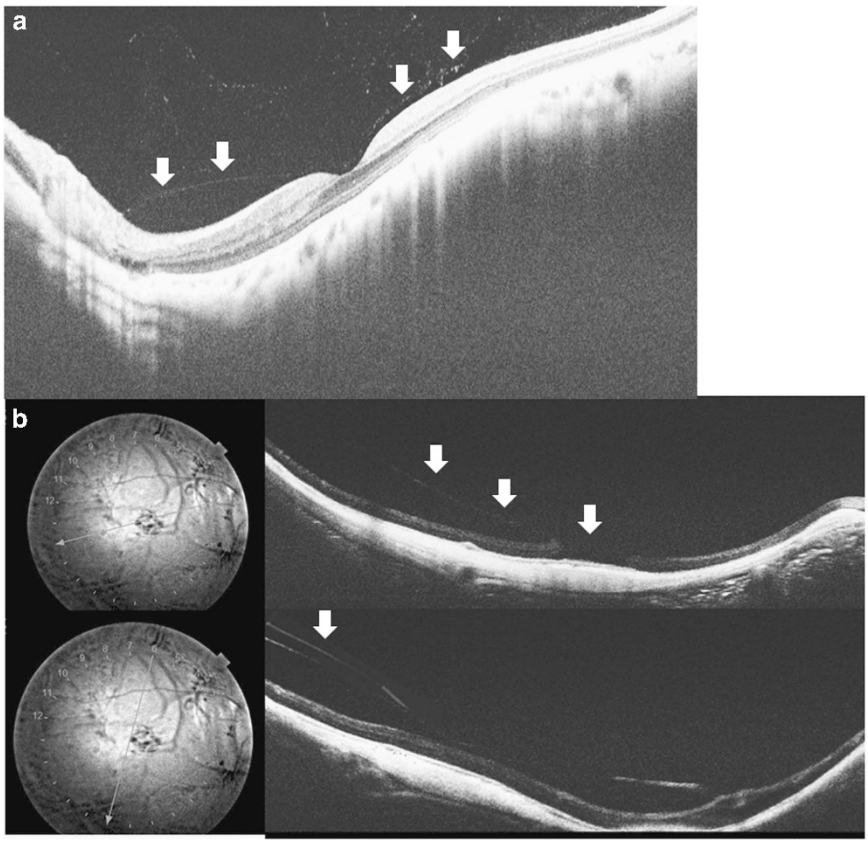

Figure 1 Optical coherence tomography scans of abnormal vitreoretinal interface. (a) Swept source OCT (SS OCT) has high penetration that allows enhanced imaging of the posterior vitreous and vitreoretinal interface (outlined by white arrows) in cross sections. The posterior wall of the posterior precortical vitreous pocket is a thin vitreous cortex attached to the retina. The curvature of the inner sclera of this highly myopic eye is asymmetrical around the fovea. There is posterior vitreous detachment in the paramacular region just above the steepest point of the curvature and extending toward the perifovea. (b) SS OCT images of a highly myopic eye with the location of the cross sections indicated by the straight line lying on the infrared fundus photos on the left side. Top: a full-thickness macular hole with parafoveal vitreous traction (white arrows) in myopic traction maculopathy. Bottom: another cross-sectional OCT image of the same eye revealed vitreoschsis (white arrow).

vitreomacular traction was due to anteroposteriorly oriented vitreous fiber exerting direct traction to the fovea.

Retina

Contrary to histopathological findings of thinned sclera and retina in myopic eyes, earlier generations of OCT did not identify any association between mean macular thickness and axial length of the eye.[22–24] Lam *et al*[25] used TD OCT with higher axial scanning resolution and sampling density, and demonstrated that there were regional variations of retinal thickness within the macular region that correlated with axial length. The outer ring macular thickness was found to be reduced with longer axial length, while the inner ring macular thickness increased with axial length. The absence of large blood vessels and optic fibers could render the peripheral retina less resistant to traction and stretch, and the decrease in peripheral retinal thickness may compensate for the stretching force over the entire retina to preserve the central retinal thickness. This finding is confirmed in population-based study in which retinal thinning with increasing axial length occurs in the outer macular regions but not in the central macular.[26]

Recently, Liu *et al*[27] used ultrahigh-resolution OCT to analyze the intraretinal structure changes in myopic eyes and developed automated layer segmentation algorithms to study the thickness of different intraretinal layers. In the central macular region, only the outer segment of the receptor layer (outer plexiform layer, myoid, and ellipsoid zones) was thickened with increased axial length. In the pericentral and peripheral regions, all layers except the ganglion cell and inner plexiform layer were found to have thickness changes in high myopia. The total thickness of the peripheral region was significantly less compared with emmetropic controls mainly due to thinner inner nuclear layer, combined Henle fiber, and outer nuclear layer. Clinicians should be aware of the pattern of regional and intraretinal variations of macular thickness in myopia subjects when interpreting the significance of a particular macular thickness in aiding diagnosis and monitoring of diseases such as diabetic macular edema or glaucoma in myopic patients.

Nevertheless, magnification as a result of change in refractive power and axial length of the eye can affect the OCT scanning radius.[23] Magnification is not routinely corrected in retinal thickness measurements in commercially available OCT instruments, thus resulting in under or overestimations in the measurement of macular thickness. Furthermore, the current normative databases in commercially available OCT systems have not taken into account the axial length of high-myopia subjects. Clinicians should be aware of the pattern of regional and intraretinal variations of macular thickness in subjects with high myopia when interpreting the macular thickness changes for diagnosing and monitoring of diseases such as diabetic macular edema or glaucoma in myopic patients.

Choroid

The choroid is a primarily vascular structure responsible for delivery of blood and nutrients to the outer retina, thermoregulation of the retina and secretion of growth factors. Given its unique position between the retina and sclera, the choroid may be a source of scleral growth regulators in response to such local visual stimuli, making it potentially important in emmetropization and axial elongation.[28] The advent of high-resolution SD OCT enabled the evaluation of choroidal biometry *in vivo*, elucidating important information regarding the choroid in human myopia progression and susceptibility to pathologic myopia. In general, there was good inter-system reproducibility of choroidal thickness measurements between EDI OCT and SS OCT and also between three different SD OCT devices: Cirrus HD OCT, Spectralis SD OCT, and RTVue.[29,30] Large population-based studies found significant correlation between increased age and increased axial length with decreased choroidal thickness.[30–34] Furthermore, the diminution in choroidal thickness with age was approximately the same in absolute quantities in highly myopic eyes as in eyes without high myopia.[35] When highly myopic eyes grow with age, the choroid may become very thin and even completely absent. Chorioretinal atrophy (CRA) in high-myopic eyes appeared white in fundoscopy due to overlying RPE hypoplasia and the underlying sclera became readily visible.

Subfoveal choroidal thickness in high myopia was found to be consistently correlated with visual function.[35–37] Studies evaluating the choroid in myopic eyes using ultrasonography and indocyanine green angiography (ICGA) demonstrated that the density of choroidal vasculature and circulation were reduced.[38–40] It is hypothesized that in the process of globe elongation in axial myopia, the choroid may well be stretched without development of additional vasculature. Progression of choroidal thinning continues with age until some point the choroid would have difficulty in supplying enough oxygen and other metabolites. The compromised choroidal circulation may account, in part for the visual function loss that is seen in high myopia.

In emmetropic eyes as well as myopic eyes, the choroidal thickness varied topographically within the posterior pole. The choroidal thickness was noted to be thinner in the inferior and nasal macula as compared with the superior and temporal macula.[33,41–43] In high-myopic eyes, the topographic difference was even more pronounced.[33,41] The reason for such topographic

variations in choroidal thickness is not fully understood and this might be related to the regional differences in the metabolic demands of the retina, pattern of choroidal vasculature distribution, and position of choroidal watershed zones. Furthermore, EDI and SS OCT have revealed intrachoroidal cavitation (ICC) that is typically located immediately inferior to the optic nerve in highly myopic eyes[44,45] (Figure 2). It was also known as peripapillary detachment or choroidal schisis.[46,47] One study reported that ICC was found in 4.9% of high-myopic eyes.[47] The overlying retina, RPE and Bruch's membrane complex remained intact over the region of ICC. This cavitation was created by expansion of the distance between the inner wall of the sclera and the posterior surface of Bruch's membrane. The process of deformation of sclera during staphylomatous expansion at the inferotemporal portion of the disc in axial myopia may have resulted in the cavitation in the choroid.[45] ICC has been reported in the macular region of high myopes and fluid may dissect through the defect underneath the retina resulting in localized retinal detachment (RD)[48] (Figure 2b).

Sclera and staphyloma

In the process of axial myopia development in humans, there is expansion of the volume of vitreous cavity as well as the surface area of the posterior sclera. The scleral wall thickness decreases, curvatures change, emissary openings widen, and the scleral canal can be enlarged, becomes tilted, and distorted. There is also local exacerbation of ocular expansion manifested as regional out-pouching, which is known as staphyloma. Curtin[49] studied the fundoscopy findings of staphyloma formation in myopes and classified them into 10 different patterns. Nonetheless, the Curtin classification is not exhaustive of all types of staphyloma. More recently, Moriyama *et al*[50] used high-resolution MRI and three-dimensional (3D) rendering to identify additional configurations of staphyloma. 3D MRI has the ability to image the entire width of the staphyloma, which may not fit into the maximum length of an OCT scan. Sometimes, the steepened curve of the posterior sclera caused by axial elongation may be confused with a staphyloma in some of the OCT studies.[51–54] Nevertheless, images obtained from T2-weighted MRI represented the fluid-filled chamber in the eye, which was not exactly the contour of the outer shell of the eye. OCT can be useful in studying the biometrics of the sclera, detecting more minute and subtle deformities within the staphyloma, and allows the analysis of the spatial relationship between morphology of the retinal and choroidal layers with the protruded sclera.[55]

In OCT, the sclera appears as a relatively uniform, hyperreflective structure exterior to the choroid. Age, axial length, presence of staphyloma, central retinal

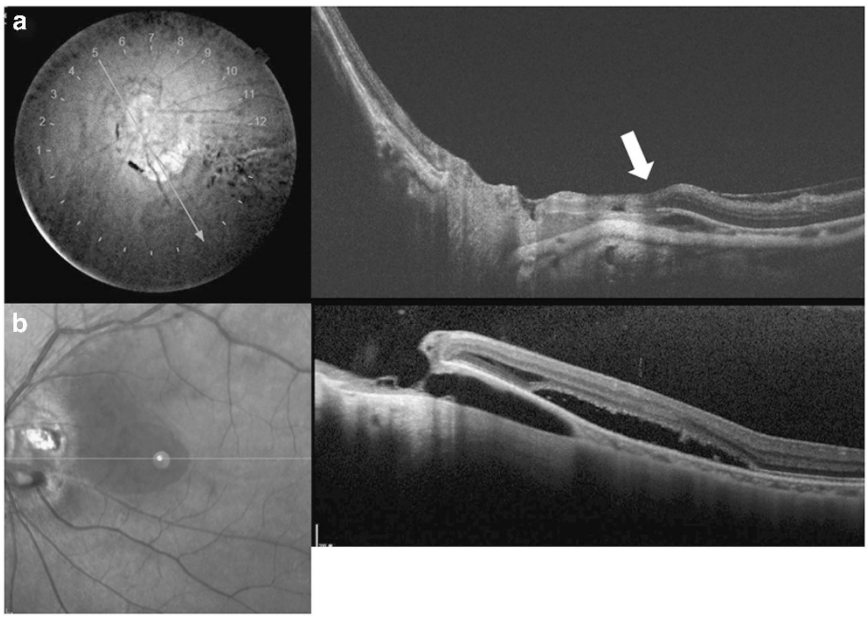

Figure 2 Optical coherence tomography (OCT) images of intrachoroidal cavation (ICC). (a) Swept source OCT slice scanned along the line lying on the infrared fundus photo (left) shows ICC below the optic nerve. Hyporeflective space (white arrow) suggesting an existence of fluid is observed within the ICC. (b) Enhance depth imaging spectral domain OCT revealed a macular retinal detachment associated with ICC. During enlargement of the ICC in a highly myopic eye, the overlying retinal tissue develops a full-thickness defect, allowing the vitreous cavity to communicate directly with the cavity of the ICC. Macular retinal detachment occurs when the communication extends into the subretinal space.

thickness, and choroidal thickness were associated with the visibility of the scleral layer by OCT.[55,56] A head-to-head comparative study reported that the detection rates of posterior border of the sclera were 67% using EDI OCT and 78% using SS OCT, but in eyes with myopia the detection rates dropped to 31% with EDI OCT and 53% with SS OCT. Therefore, SS OCT is preferred over EDI OCT for imaging of the sclera.

Subfoveal scleral thickness in highly myopic eyes using OCT has only slight variation between EDI OCT, SS OCT, and histological studies.[55,57] Ohno-Matsui *et al*[55] studied 488 highly myopic eyes with both 3D MRI and SS OCT and they found that the most protruded part of the sclera existed along the visual axis in 78% and inferior to the central axis in 22%. The sclera in the lower half of the eye is the area where the embryonic ocular fissure closes, and it may be possible that this part of the sclera is structurally weaker and more susceptible to elongation. Four patterns of curvatures of the inner sclera were observed: curvatures that sloped toward the optic nerve, symmetrical and centered on the fovea, asymmetrical around the central fovea (Figure 1a), and irregular (without a circular arc).[55] Irregular curvature was found to be associated with older age and visual field defects with higher incidence of macular pathology including myopic traction maculopathy (MTM), myopic choroidal neovascularization (mCNV), and CRA.[55] When analyses of both 3D MRI images and SS OCT were combined, eyes with temporally dislocated staphyloma might represent a condition in which the sclera was extremely thin and became the irregular curvature shown by SS OCT.[58] This finding was also correlated with the steeply curved staphyloma observed by stereoscopic fundus photography.[55] It is hypothesized that in highly myopic eyes, the thinned sclera may no longer maintain the integrity of the globe and results in irregular curvature, which may potentially cause abnormal stresses on RNFL and vitreomacular interface predisposing to visual threatening conditions.[55]

Emissary blood vessels ordinarily penetrate the eye, often at oblique angles, and course through the sclera toward the choroid. With elongation of the eye and stretching of the sclera, these passageways may become much shorter and their openings also become stretched. The drainage of choroidal veins is mainly though the vortex system that exits the sclera at the equatorial region of the globe. Previous ICGA study suggested that choroidal venous blood is also drained around the macula in highly myopic eyes but was unable to be confirmed by using computer tomographic angiography because of its relatively low resolution.[59] Using SS OCT, the entire course of a macular vortex vein running through the choroid until its exit from the sclera could be observed.[60] SS OCT was also able to image the lateral long posterior ciliary artery, short posterior ciliary arteries, and some retrobulbar blood vessels, which was confirmed by ICGA findings.[55] Nevertheless, deep vessels and structures were only visible in eyes when the amount of CRA was severe. Future longitudinal studies are necessary for the understanding of how alterations of intrascleral vascular structures are related to the development of chorioretinal complications or optic nerve damages in patients with pathologic myopia.

Dome-shaped macula

In 2008, Gaucher *et al*[61] first described dome-shaped macula as inward bulge of the macula within the concavity of a posterior staphyloma in highly myopic eyes based on OCT observations. Subsequently, with the use of EDI OCT, Imamura *et al*[62] reported that dome-shaped macula was the result of a localized variation in thickness of the sclera in the macular area. Caillaux *et al*[63] further used SD OCT and 3D reconstructions to classify the morphology of dome-shaped macula include round-shape, horizontal oval-shape, and vertical oval-shape. The authors recommended both vertical and horizontal OCT scans to be performed in order to avoid overlooking a dome-shaped macula.

There are still many uncertainties regarding dome-shaped macula. Postulations for the exact mechanism for its development include: resistance to deformation of scleral staphyloma, scleral infolding through the collapse of the posterior portion of the eye wall, and tangential vitreoretinal traction. There is no population-based study that reported its prevalence, and it is unclear whether various macular complications reported to occur in eyes with dome-shaped macula are unique to it or are common complications of highly myopic eyes regardless of the presence of dome-shaped macula. Visually threatening macular complications have been suggested to be more frequent in eyes with dome-shaped macula than eyes with low or no myopia, which include serous RD, mCNV, macular holes (MHs), and foveal and extrafoveal schisis.[64] Liang *et al*[65] reported the largest cohort of 1118 highly myopic eyes and found 225 (20.1%) eyes had a dome-shaped macula. Younger age and longer axial length were positively associated with the presence of dome-shaped macula. The most common morphology was the vertically oriented subtype (77.3%), followed by the bidirectional (20.1%) and horizontal subtype (2.6%) (Figure 3). The rates of foveal and extrafoveal retinoschisis and serous RD were significantly associated with the presence of a dome-shaped macula. Nevertheless, the rate of serous RD was highly variable among different studies, ranging from 1.7 to 52.1% due to possible selection bias.[65] mCNV had been reported to be another frequent complication of dome-shaped macula, with range of 12.2–47.8%.[65] Nevertheless, Liang *et al*[65]

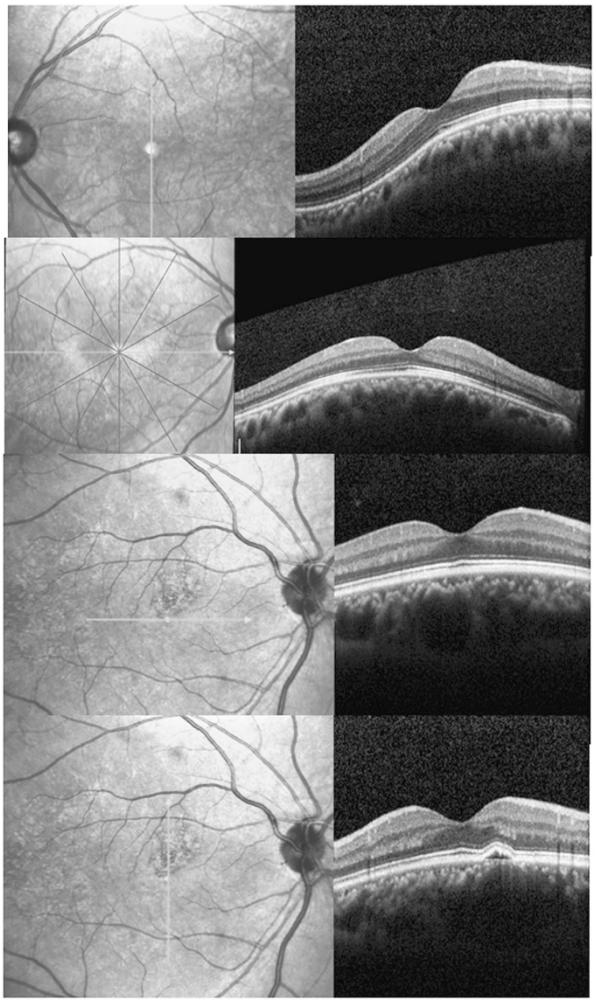

Figure 3 Cross section enhanced depth imagining spectral domain OCT images with their orientation indicated by the thick straight lines lying on the left side fundi images. Top: vertically oriented dome-shaped maculopathy. Second from top: horizontally oriented dome-shaped maculopathy. Third from top and bottom: a bidirectional type dome-shaped maculopathy. A small juxtafoveal pigmented epithelial detachment is shown in the vertical orientation.

performed multivariate analyses and showed that the overall rate of mCNV was significantly associated with age but not with the presence of dome-shaped macula.

Optic nerve head

The anatomic changes in the optic nerve head and surrounding structures in high myopia are becoming more readily evident by OCT imaging. There is altered mechanical stress on the nerve fibers and compromised prelaminar perfusion in myopic eyes. However, the functional changes induced by the structural changes and the possible pathophysiologic mechanisms are still being researched.

Tilting of the optic nerve is more common among high myopes in large population-based studies.[66] The terminology used for describing a tilted disc is a misnomer, as it refers to the optic disc being rotated in the transverse plane from a two-dimensional fundoscopic view. In the process of globe elongation, there are three possible axes of rotation for the optic nerve head: horizontal axis, vertical axis, and torsional axis. Usually, the temporal portion of the nerve is more posterior than the nasal portion. In the past, there was an attempt to measure the angle of optic disc tilting by measuring the ratio between the minimum and maximum diameter of the optic nerve in fundus photo. However, this index was not comparable among patients because the optic disc dimensions measured in fundus photography may not be the true dimensions of the optic discs.[67] The true angle of tilt can now be measured using OCT.[68]

Although the size of optic discs in normal eyes showed significant variation, its relationship with axial length and myopia is still a matter of contention. Two groups of investigators using SD OCT reported an inverse correlation between optic discs size with either refractive error or axial length, but the authors did not perform image size corrections for magnification variations.[69,70] In a population-based study, Jonas and colleagues[71] divided those with large optic discs into primary and secondary subtypes. The primary macrodiscs had no relationship with refractive error while the secondary type, generally observed in refractive error of − 8D or greater, had increasing size with increasing myopia. Enlargement of the optic nerve head in high myopes occurred due to expansion and stretching of the scleral canal and the lamina cribrosa. OCT was able to observe the acquired pits of the optic nerve, dehiscence of the lamina cribrosa, expansion of the dural attachment posteriorly with enlargement of the subarachnoid spaces immediately behind the eye and expansion of the circle of Zinn-Haller, with potential compromised circulation into the prelaminar portion of the optic nerve (Figure 4).

OCT was able to image the dilated subarachnoid space around the exit of the optic nerve in highly myopic eyes *in vivo*. The subarachnoid space was triangular, with the base toward the eye surrounding the optic nerve in the region of the scleral flange. Hypothetically, the expanded area of exposure to cerebrospinal fluid pressure along with thinning of the posterior eye wall may influence staphyloma formation and the pathogenesis of glaucoma.

Similar to the abnormal expansion in size of the scleral emissaries, analogous abnormalities have been observed in the region centered around the optic nerve. Using SS OCT, Ohno-Matsui *et al*[55] observed pit-like changes in the region of the conus similar to those in the macular region in 16.2% of highly myopic eyes. There was absence of RNFL tissue overlying the pits, and this discontinuity

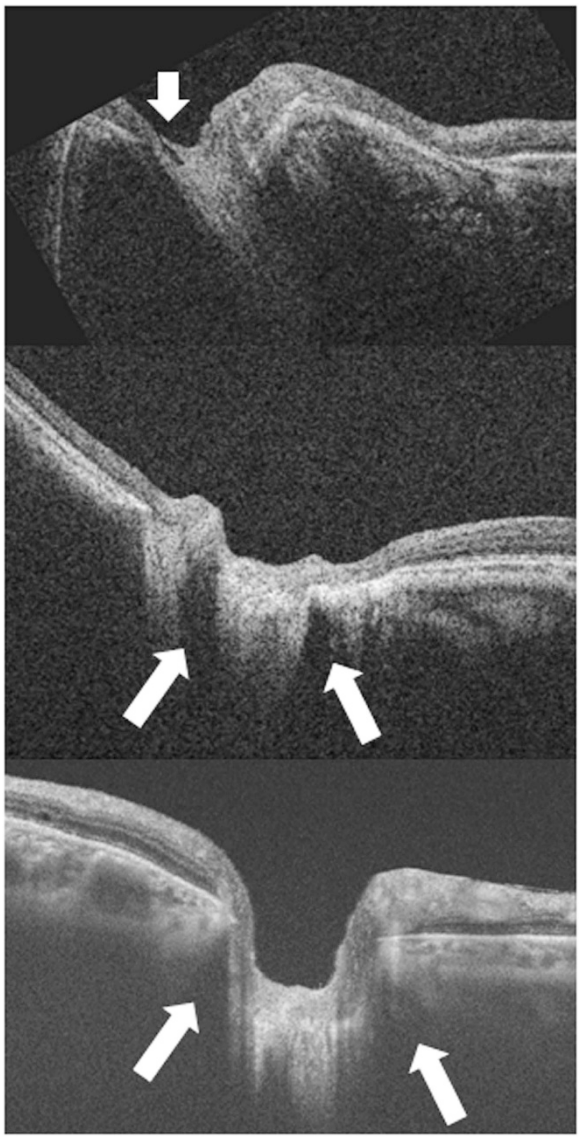

Figure 4 Enlargement of the optic nerve head in highly myopic eyes occurs due to stretching of the scleral canal and lamina cribrosa. The lamina is torn from the peripapillary sclera and eventually the overlying nerve fiber is disrupted, and this stage is observed as optic disc pits, especially at the superior and inferior poles of the optic disc. Top: optical coherence tomography (OCT) shows a hyporeflective gap indicating the acquired pit of the optic nerve (white arrow). Middle: OCT shows the subarachnoid spaces as hyporeflective triangular spaces along both the upper and lower borders of the optic nerve (white arrows). The elongated dural attachment at posterior scleral canal in highly myopic eye leads to widening of retrobulbar subarachnoid spaces comparing with that observed in an ametropic eye (Bottom).

may account for visual field defects observed in highly myopic eyes.

The peripapillary region of large optic discs secondary to high myopia invariably has prominent parapapillary atrophy that involves the choroid, RPE, and outer retina. Furthermore, rotations of the optic nerve are expected to cause a shift of RNFL entering the optic nerve head. In these eyes, the automatic segmentation protocols used in commercially available OCT machines could not accurately measure the thickness of the RNFL, and therefore highly myopic patients were among the most difficult patients to evaluate for glaucoma[7,72,73] (Figure 5). The pattern of RNFL distribution was altered in high myopes with thinner average, superior, nasal, and inferior but thicker temporal nerve fiber layer thickness and a temporal shift in the superior and inferior peak locations.[73] Torsion of the optic disc occurs when it is rotated along the coronal plane, and the direction of rotation is more commonly counterclockwise such that the superior aspect of the long axis is rotated temporally when viewing the right eye. The RNF from the temporal periphery courses around the central macula, converging on the optic canal either superiorly or inferiorly. Using Cirrus SD OCT, Leung *et al*[7] measured the angle between the superotemporal and inferotemporal RNFLf bundles, and reported decreasing magnitude of the angle with increasing axial length. As the normative database of the Cirrus OCT largely comprises data collected from normal eyes with no or low myopia, interpreting RNF layer thickness deviation maps in highly myopic patients was likely to be inaccurate. An alternative could be to measure the cell bodies instead of the axons. The ganglion cell complex can be visualized, segmented, and measured in eyes by SD OCT, but further longitudinal, large-scale studies are necessary to validate its translation into clinical practice.[74–76]

Myopic traction maculopathy

The term MTM was proposed by Panozzo and Mercanti[77] in 2004 to unify all of the abnormal OCT features generated by traction in pathologic myopia. Although some of the clinical manifestations of MTM might be observed on ophthalmoscopic exam, OCT is necessary for its diagnosis. Eyes with MTM include those with vitreomacular traction (Figure 1a), epiretinal membrane, macular retinoschisis, lamellar MH, and MH (Figure 1b) with or without RD. Using SD OCT, macular retinoschisis could be observed as the splitting of the inner retina from the outer retinal layers with multiple columnar structures connecting the split retinal layers.[78] The splitting of the outer retina appeared to occur between the outer plexiform layer and the outer nuclear layer.[78] The columnar structures corresponded to the retention of the Henle's nerve fiber layer. Retinoschisis may also be present at the level of the inner plexiform layer or an inner limiting membrane (ILM) detachment.[78] Macular RD may sometimes coexist with macular retinoschisis, which may also be accompanied by an outer lamellar MH.[79]

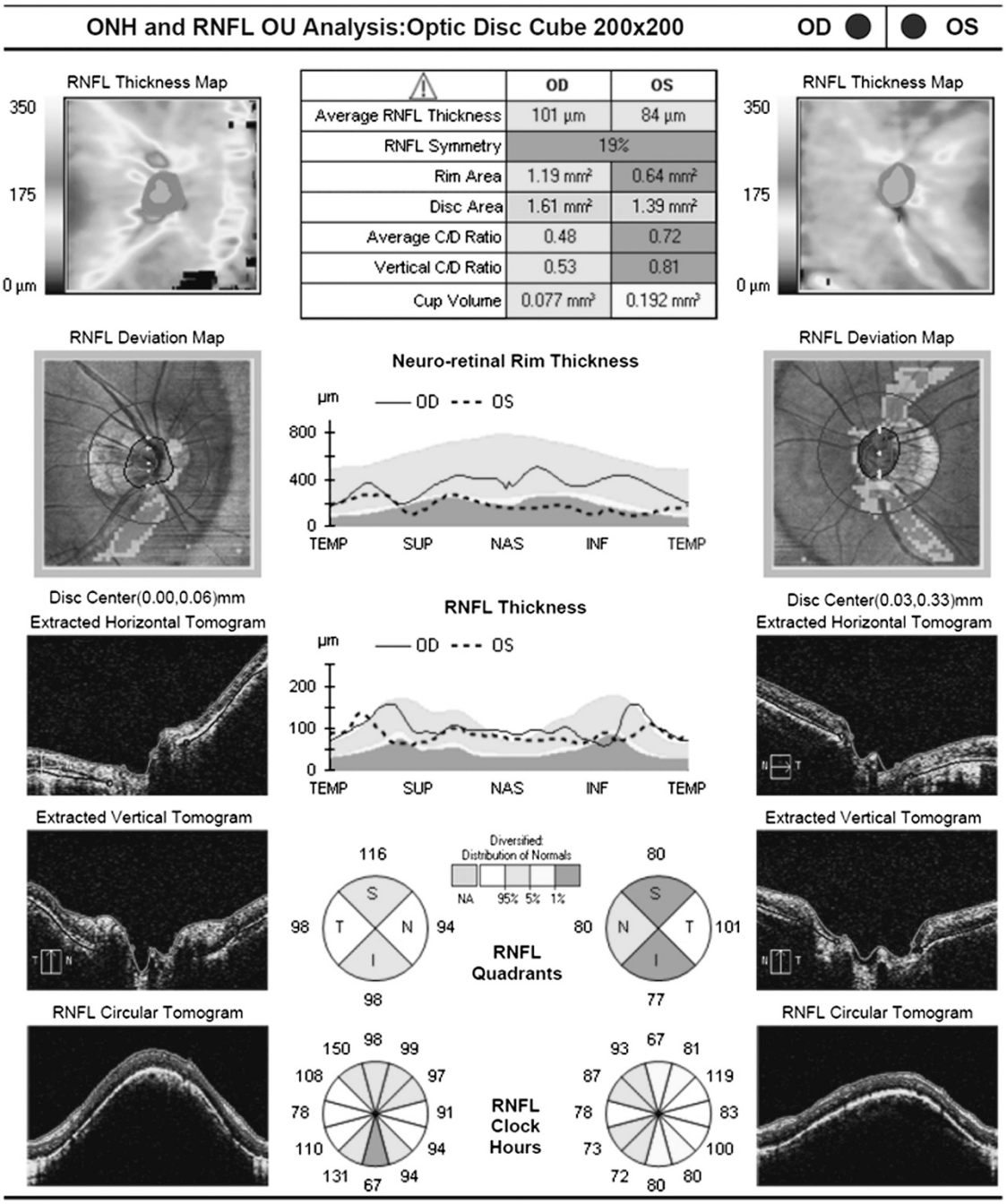

Figure 5 Retinal nerve fiber layer (RNFL) analysis by Cirrus optical coherence tomography (OCT) shows abnormally reduced thickness in inferior sector of the right eye and superotemporal and inferotemporal sectors in the left eye of a high myopia patient. In glaucoma eyes, there is predilection of inferior and superior RNFL loss. However, the normative database of Cirrus OCT only comprises data collected from normal eyes with no or low myopia. The interpretation of RNFL thickness deviation may need to account for its altered topographical distribution in highly myopic eyes.

The occurrence of MTM was associated with increased axial length and macular CRA. Recent studies using SS OCT have evaluated the relationship between scleral curvature alterations and the pathogenesis of MTM. Ohno-Matsui *et al*[48] demonstrated that eyes with macular retinoschisis more frequently had ICC in the macular area with patchy CRA, and the sclera immediately underneath the ICC was bowed posteriorly. Sclera with an irregular inner curvature more commonly had macular retinoschisis. These observations suggested that the scleral contour affects the development of MTM. Furthermore, OCT showed paravascular abnormalities including

paravascular lamellar holes, vascular microfolds, and paravascular retinal cysts in eyes with MTM[80] (Figure 6). Glial cells that exist abundantly around the retinal vessels can migrate and proliferate through the paravascular lamellar holes to produce collagen and facilitate the proliferative and contractile response of ILM.

Shimada *et al*[81] observed MTM eyes longitudinally with OCT and proposed that the progression from macular retinoschisis to RD passed through four stages: (1) a focal irregularity of the thickness of external retina, (2) an outer lamellar MH development within the thickened area and subsequent development of small RD, (3) horizontal separation of the column-like structures overlying the outer lamellar hole and vertical enlargement of outer lamellar hole, and (4) elevation of the upper edge of the external retina and the attachment to the upper part of retinoschisis layer accompanying with further enlargement of RD. Shimada *et al*[81] also analyzed the largest cohort of MTM eyes to-date with follow-up of more than 24 months and reported their variable natural courses. Of the 207 eyes, 11.6% experienced progression of MTM, and eyes with more extensive macular retinoschsis were at significantly higher risk for progression. Around 4% of eyes showed a decrease or complete resolution of the macular retinoschisis, which may occur after spontaneous release of traction on the retina. In another study on the natural history of MTM, Tanaka *et al*[82] reported that the presence of a lamellar MH might be a relatively stable condition in MTM eyes.

The indication and the optimal timing for pars plana vitrectomy (PPV) in MTM eyes without RD is unknown. Shimada *et al*[79] recommended surgery in macular retinoschisis eyes between stage 3 and 4, because delayed PPV (in stage 4) has the increased risk of developing full-thickness MH postoperatively. The need for ILM peeling is also controversial. ILM peeling is indicated when apparent ILM traction is recognized on OCT to prevent postoperative recurrence of MTM.[83] However, ILM peeling may increase the risk of postoperative full-thickness MH, because peeling may induce breaks within the already thinned and weakened central foveal tissue.[84] A fovea-sparing ILM peeling technique has been proposed, which enabled release of macular traction, reduced risk of surgical trauma to the central fovea, and centripetal contraction of the remaining ILM to prevent postop MH formation.[85] Posterior scleral reinforcement surgery, intraocular expansible gas, and prone posturing has been reported to treat macular retinoschisis in MTM.[86] OCT is also an indispensable tool for monitoring of postoperative MTM patients (Figure 7).

Other types of MH and RDs in pathologic myopia

MH has been observed at the border between an old CNV and the surrounding CRA in which RD developed in 89% of eyes with complete PVD, and therefore, the mechanism of MH may not be completely due to vitreomacular traction.[87] Macular RD has been observed in highly myopic eyes with peripapillary intrachoroidal cavity.[87] OCT revealed the communication between the ICC with vitreous cavity through a full-thickness tissue defect in the

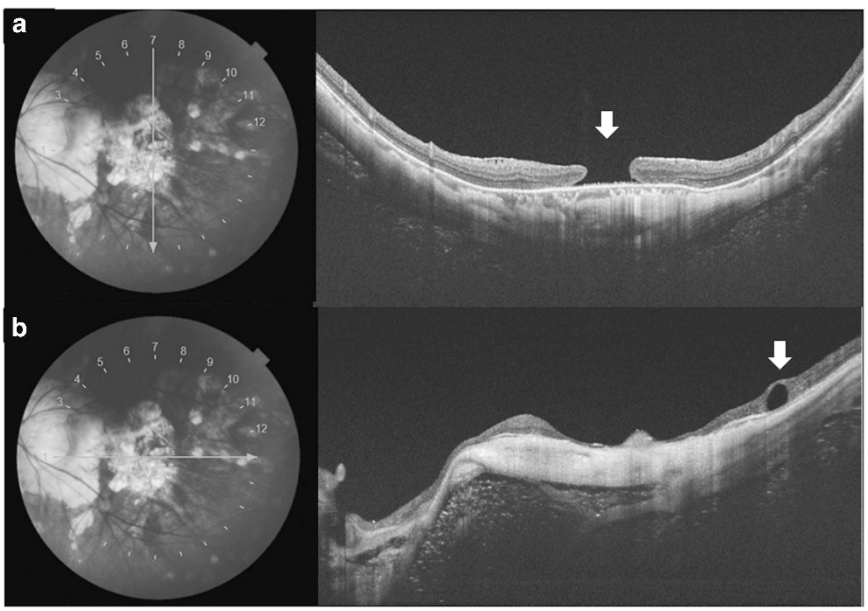

Figure 6 Optical coherence tomography (OCT) scans of myopic traction maculopathy (MTM). (a) A patient with MTM developed full-thickness macular hole (white arrow) in swept source OCT. (b) A horizontal OCT slice of the same eye revealed a paravascular retinal cyst (white arrow) associated with MTM.

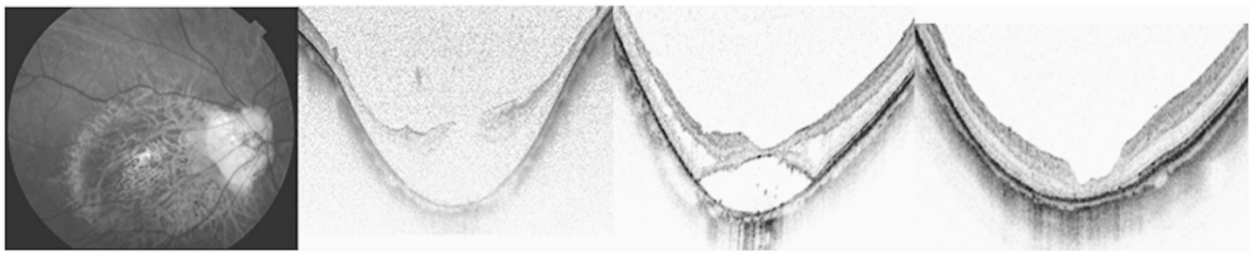

Figure 7 Left: fundus photo of the posterior staphyloma and chorioretinal atrophy. Second from left: spectral domain optical coherence tomography (SD OCT) reveals retinoschisis with MH. Note that the sclera is strongly bowed posteriorly and the curve is symmetrical around the fovea. The patient underwent posterior vitrectomy with internal limiting-membrane peeling and gas tamponade. Third from left: SD OCT 3 months post operation shows that the macular gradually flattened. Right: SD OCT at 4 years after operation. The MH remains closed.

overlying retina into the subretinal space, which may be associated with macular RD.

As for macular retinoschisis, there is no standard technique for treatment of MHRD. In general, the surgery proposed for MHRD is vitrectomy, removal of adherent vitreous cortex, removal of ERM, fluid–gas exchange, and intraocular gas or silicone oil tamponade. Kuriyama *et al* reported the inverted ILM flap technique in which the ILM was not removed completely from the retina during vitrectomy but was left attached to the edge of the MH.[80] The ILM was then massaged gently over the MH so that the MH was covered with the inverted ILM flap.

Myopic choroidal neovascularization

In patients with mCNV, OCT can show exudative features including intra- or subretinal fluid, and the hyperreflective lesion located beneath the neurosensory retina representing the mCNV. The mCNV can cause the contour of the RPE monolayer to elevate. Small hemorrhages are usually not easy to visualize with OCT, which may also be associated with lacquer crack instead of the CNV. Because of the typically minimal amount of exudation associated with myopic CNV, the presence of subretinal or intraretinal fluid in OCT may not be a sensitive and reliable imaging marker for new onset or recurrent myopic CNV.[88–91] Leveziel *et al*[90] compared the use of FA with OCT in a cohort of 90 eyes for the detection of new onset mCNV and reported that FA leakage was observed in 82% of cases, while exudative sign on SD OCT was only observed in 48.6% of cases. These findings suggest that FA may be more sensitive in the diagnosis of active mCNV and the confirmation of active myopic CNV still largely relies on dye leakage detected in FA.[90,91] The discordance between FA and SD OCT findings has not been clearly reported in CNV associated with age-related macular degeneration.[92] Nonetheless, SD OCT are useful in detecting various differential diagnoses of mCNV which include MH, small focal areas of CRA or scarring, and inflammatory conditions such as multifocal choroiditis and panuveitis and should be included in the standard of care of managing mCNV.[93] High myopes frequently have small areas of altered pigmentation in the posterior pole. Small hyperpigmented spots are usually flat and do not have a surrounding area of atrophy. True CNV causes an elevation at the level of the RPE. Multifocal choroiditis and panuveitis cause grayish-white inflammatory lesions at the level of the RPE that can have associated subretinal fluid during the acute, active phase.[94] OCT shows the inflammatory lesions to be conical elevations of the sub-RPE.[94] Clues that the eye harbors multifocal choroiditis are multiple lesions in the fundus with clinically evident inflammatory cells.

Intravitreal injection of anti-vascular endothelial growth factor (anti-VEGF) is the current treatment of choice for mCNV patients and OCT was indicated in the RADIANCE and MYRROR studies, both multicenter randomized controlled Phase III trials for the monitoring of disease activity after treatment[95,96] (Figure 8). When a treated lesion shows cessation of activity, the lesion becomes more compact, the internal reflectivity is often less than the surface, the boundary between the lesion and retina is sharp, and there is no associated intra- or subretinal fluid. When the lesion becomes active, any of these parameters may change. Besides baseline visual acuity, size of the CNV and the presence of CRA, the subfoveal choroidal thickness have been shown to be prognostic factor of mCNV recurrence. It is possible that reduced choroidal blood flow in the subfoveal area predispose to the development of mCNV.[97] Recently, subretinal hyperreflective exudation imaged by OCT in mCNV patients has been suggested in monitoring response to anti-VEGF agents by both qualitative (regression) and quantitative (thickness) assessments. The typical type 2 CNV in pathologic myopia grows under the RPE and penetrates the Bruch membrane to extend into the subretinal space, which may facilitate the deposition of these hyperreflective lesions into the subretinal space.[98] The presence of a subretinal hyperreflective exudation on SD OCT could help in assisting the decision on whether to perform FA or not, and making decision on retreatment.

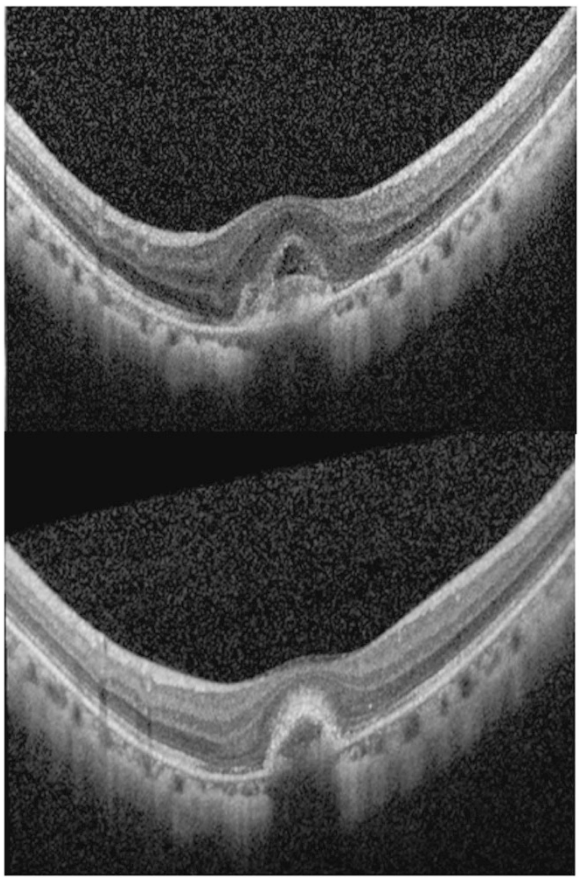

Figure 8 Optical coherence tomography (OCT) scans of myopic choroidal neovascularization (CNV). Top: SD OCT reveals intra- and subretinal fluid associated with an active myopic CNV. Bottom: after treatment with intravitreal anti-VEGF injection, there is resolution of both intra- and subretinal fluid. The lesion becomes more compact and the boundary between the lesion and retina becomes apparent.

Nevertheless, multimodal imaging is necessary to distinguish it from other causes of hyperreflective subretinal lesions such as hemorrhage and fibrosis. The subretinal hyperreflective exudation correlates to the fundus photography observation of a subtle yellowish material deposit and autofluorescence imaging showing it as an isoautofluorescent lesion.

Myopic maculopathy and CRA

Myopic maculopathy was characterized by ophthalmoscopic findings of various retinal and choroidal lesions associated with excessive axial elongation of the globe. Owing to a lack of common classification scheme, a direct comparison of the incidence or prevalence and the burden of myopic maculopathy in epidemiological studies has not been possible. Hence, an international classification and grading system for myopic maculopathy was published by the meta-analysis for pathologic myopia study group in 2015.[99] The new system adopted the fundus photo classification based on long-term observational studies that is reliable and convenient. It has five categories of myopic maculopathy including: no myopic retinal degenerative lesion, tessellated fundus, diffuse CRA, patchy CRA, and macular atrophy. Three additional 'plus' features were lacquer cracks, mCNV, and Fuchs spot. A posterior staphyloma may or may not be limited to the macular area and its grading is considered in a separate category.

Spaide analyzed the features of tessellated fundus with EDI OCT and reported reduction of mean choroidal thickness.[100] Attenuation of choroid might occur with RPE hypoplasia that allows the underlying choroidal vessels to be more visible, thereby causing the appearance of tessellated fundus. The attenuation is one of the earliest visible signs in eyes with high myopia, which begins to develop around the optic disc and the area between the optic disc and the central fovea. Lacquer cracks are fine, irregular yellow lines, often branching, and crisscrossing. OCT may detect the discontinuity of Bruch's membrane and the underlying increased penetrance.[101] Nonetheless, it is seldom visualized by OCT because lacquer cracks are narrow. Diffuse CRA is an ill-defined yellowish-white atrophy on fundus photography. OCT shows marked thinning or even absence of choroid in the area of diffuse CRA. Large choroidal vessels may be observed to protrude toward the retina. It is interesting to observe that even in area where most of the choroidal layer is absent, the outer retinal layer may still be present. This might explain the relatively preserved vision in some eyes with diffuse myopic CRA.[100] When diffuse CRA is only present around the optic disc, OCT is useful in differentiating CRA from peripapillary ICC because of their similar ophthalmoscopic appearance.[45]

Patchy CRA is represented by a grayish-white well-defined atrophy on fundus photo. Based on long-term natural course study of eyes with pathologic myopia, three types of patchy atrophy were observed: patchy atrophy that develops from lacquer cracks, patchy atrophy that develops within the area of an advanced diffuse CRA, and patchy atrophy that can be seen along the border of the posterior staphyloma.[102] For the first two types, OCT images show a loss of photoreceptors, RPE, and inner choroid in the area of patchy atrophy in the macular area, while the inner retina appeared to be attached directly to the sclera.[48] Hence, despite the loss of outer retinal tissue, the inner retinal layer is maintained in the area of patchy atrophy. A recent OCT study that evaluated patchy atrophy along the edge of posterior staphyloma has revealed severe thinning of both inner and outer retinal layers, which was not observed in the two other types of patch atrophy.[103] It could be possible that the entire retina is bent and thinned along

the steep edge of the staphyloma, which predisposes the development of patchy CRA and subsequently the inner retina may be disrupted mechanically. There is also visual field defect corresponding to the course of the RNF layer across the area of patchy atrophy. Nevertheless, it is not known whether such defect is due to genuine glaucoma, or due to the disruption of the nerve fibers overlying the patching atrophy, or caused by refractive scotoma.[103]

A well-defined patch of CRA may develop around the scarred mCNV with gradual enlargement. OCT cannot differentiate between the atrophy stage of mCNV and patchy atrophy. Their main difference is that CRA associated with late stage of mCNV is located relatively close to the central fovea and enlarges circumferentially around the fovea. In contrast, patchy atrophy rarely involves the fovea.

In anticipation of the wide-spread application of OCT imaging technology, OCT characteristics might be added to the classification system of myopic maculopathy in the future as retinal and choroidal thicknesses appeared to be useful in evaluating CRA attributable to pathologic myopia. This can provide a more objective, quantitative, and comprehensive assessment tool for epidemiologic studies and for therapeutic clinical trials.

Future development

Even though OCT instruments have been improving over time, the extreme axial length of highly myopic eyes still represents challenges for imaging. The posterior portion of a highly myopic eye often has staphyloma and curvatures of the eyewall appear exaggerated in OCT renderings. The zone in which the images are obtained in most commercial OCT instruments is ~2 mm. Ultra-wide scans can be utilized to image the full extent of a highly myopic eye and the entire posterior inner curvature.[104] En-face OCT can provide topographical assessments of the posterior segment with quantitative point-to-point localized assessment of changes.[105] En-face OCT-assisted surgery in myopic eyes with MH can facilitate the removal of premacular tractional structures. Ultra-long scan depth OCT is currently under development to image the entire eye.[106] Because of its high resolution, high scan speed, and convenience, it has the potential to replace 3D MRI in the evaluation and classification of posterior staphyloma. Finally, OCT angiography will enable the study of blood vessels remodeling and perfusions in high-axial myopia.[107]

Conflict of interest

The authors declare no conflict of interest.

Acknowledgements

The work has not been previously presented.

References

1 Resnikoff S, Pascolini D, Mariotti SP, Pokharel GP. Global magnitude of visual impairment caused by uncorrected refractive errors in 2004. *Bull World Health Organ* 2008; **86**(1): 63–70.
2 Saw SM, Katz J, Schein OD, Chew SJ, Chan TK. Epidemiology of myopia. *Epidemiol Rev* 1996; **18**(2): 175–187.
3 Liu HH, Xu L, Wang YX, Wang S, You QS, Jonas JB. Prevalence and progression of myopic retinopathy in Chinese adults: the Beijing Eye Study. *Ophthalmology* 2010; **117**(9): 1763–1768.
4 Jonas JB, Xu L. Histological changes of high axial myopia. *Eye (Lond)* 2014; **28**(2): 113–117.
5 Wong TY, Ferreira A, Hughes R, Carter G, Mitchell P. Epidemiology and disease burden of pathologic myopia and myopic choroidal neovascularization: an evidence-based systematic review. *Am J Ophthalmol* 2014; **157**(1): 9–25 e12.
6 You QS, Peng XY, Xu L, Chen CX, Wang YX, Jonas JB. Myopic maculopathy imaged by optical coherence tomography: the beijing eye study. *Ophthalmology* 2014; **121** (1): 220–224.
7 Leung CK, Mohamed S, Leung KS, Cheung CY, Chan SL, Cheng DK *et al.* Retinal nerve fiber layer measurements in myopia: An optical coherence tomography study. *Invest Ophthalmol Vis Sci* 2006; **47**(12): 5171–5176.
8 Swanson EA, Izatt JA, Hee MR, Huang D, Lin CP, Schuman JS *et al. In vivo* retinal imaging by optical coherence tomography. *Opt Lett* 1993; **18**(21): 1864–1866.
9 Spaide RF, Koizumi H, Pozzoni MC. Enhanced depth imaging spectral-domain optical coherence tomography. *Am J Ophthalmol* 2008; **146**(4): 496–500.
10 Chinn SR, Swanson EA, Fujimoto JG. Optical coherence tomography using a frequency-tunable optical source. *Opt Lett* 1997; **22**(5): 340–342.
11 Drexler W, Liu M, Kumar A, Kamali T, Unterhuber A, Leitgeb RA. Optical coherence tomography today: speed, contrast, and multimodality. *J Biomed Opt* 2014; **19**(7): 071412.
12 Kishi S, Shimizu K. Posterior precortical vitreous pocket. *Arch Ophthalmol* 1990; **108**(7): 979–982.
13 Fine HF, Spaide RF. Visualization of the posterior precortical vitreous pocket *in vivo* with triamcinolone. *Arch Ophthalmol* 2006; **124**(11): 1663.
14 Pang CE, Freund KB, Engelbert M. Enhanced vitreous imaging technique with spectral-domain optical coherence tomography for evaluation of posterior vitreous detachment. *JAMA Ophthalmol* 2014; **132**(9): 1148–1150.
15 Itakura H, Kishi S, Li D, Akiyama H. Observation of posterior precortical vitreous pocket using swept-source optical coherence tomography. *Invest Ophthalmol Vis Sci* 2013; **54**(5): 3102–3107.
16 Schaal KB, Pang CE, Pozzoni MC. Engelbert M. The premacular bursa's shape revealed *in vivo* by swept-source

optical coherence tomography. *Ophthalmology* 2014; **121**(5): 1020–1028.
17 Itakura H, Kishi S, Li D, Akiyama H. En face imaging of posterior precortical vitreous pockets using swept-source optical coherence tomography. *Invest Ophthalmol Vis Sci* 2015; **56**(5): 2898–2900.
18 Spaide RF. Visualization of the posterior vitreous with dynamic focusing and windowed averaging swept source optical coherence tomography. *Am J Ophthalmol* 2014; **158** (6): 1267–1274.
19 Novak MA, Welch RB. Complications of acute symptomatic posterior vitreous detachment. *Am J Ophthalmol* 1984; **97**(3): 308–314.
20 Gupta P, Yee KM, Garcia P, Rosen RB, Parikh J, Hageman GS *et al.* Vitreoschisis in macular diseases. *Br J Ophthalmol* 2011; **95**(3): 376–380.
21 Itakura H, Kishi S, Li D, Nitta K, Akiyama H. Vitreous changes in high myopia observed by swept-source optical coherence tomography. *Invest Ophthalmol Vis Sci* 2014; **55** (3): 1447–1452.
22 Lim MC, Hoh ST, Foster PJ, Lim TH, Chew SJ, Seah SK *et al.* Use of optical coherence tomography to assess variations in macular retinal thickness in myopia. *Invest Ophthalmol Vis Sci* 2005; **46**(3): 974–978.
23 Wakitani Y, Sasoh M, Sugimoto M, Ito Y, Ido M, Uji Y. Macular thickness measurements in healthy subjects with different axial lengths using optical coherence tomography. *Retina* 2003; **23**(2): 177–182.
24 Zou H, Zhang X, Xu X, Yu S. Quantitative *in vivo* retinal thickness measurement in chinese healthy subjects with retinal thickness analyzer. *Invest Ophthalmol Vis Sci* 2006; **47** (1): 341–347.
25 Lam DS, Leung KS, Mohamed S, Chan WM, Palanivelu MS, Cheung CY *et al.* Regional variations in the relationship between macular thickness measurements and myopia. *Invest Ophthalmol Vis Sci* 2007; **48**(1): 376–382.
26 Huynh SC, Wang XY, Rochtchina E, Mitchell P. Distribution of macular thickness by optical coherence tomography: findings from a population-based study of 6-year-old children. *Invest Ophthalmol Vis Sci* 2006; **47**(6): 2351–2357.
27 Liu X, Shen M, Yuan Y, Huang S, Zhu D, Ma Q *et al.* Macular Thickness Profiles of Intraretinal Layers in Myopia Evaluated by Ultrahigh-Resolution Optical Coherence Tomography. *Am J Ophthalmol* 2015; **160**(1): 53–61 e2.
28 Summers JA. The choroid as a sclera growth regulator. *Exp Eye Res* 2013; **114**: 120–127.
29 Branchini L, Regatieri CV, Flores-Moreno I, Baumann B, Fujimoto JG, Duker JS. Reproducibility of choroidal thickness measurements across three spectral domain optical coherence tomography systems. *Ophthalmology* 2012; **119**(1): 119–123.
30 Agawa T, Miura M, Ikuno Y, Makita S, Fabritius T, Iwasaki T *et al.* Choroidal thickness measurement in healthy Japanese subjects by three-dimensional high-penetration optical coherence tomography. *Graefes Arch Clin Exp Ophthalmol* 2011; **249**(10): 1485–1492.
31 Li XQ, Larsen M, Munch IC. Subfoveal choroidal thickness in relation to sex and axial length in 93 Danish university students. *Invest Ophthalmol Vis Sci* 2011; **52**(11): 8438–8441.
32 Gupta P, Jing T, Marziliano P, Cheung CY, Baskaran M, Lamoureux EL *et al.* Distribution and determinants of choroidal thickness and volume using automated segmentation software in a population-based study. *Am J Ophthalmol* 2015; **159**(2): 293–301 e3.
33 Harb E, Hyman L, Gwiazda J, Marsh-Tootle W, Zhang Q, Hou W *et al.* Choroidal thickness profiles in myopic eyes of young adults in the correction of Myopia Evaluation Trial Cohort. *Am J Ophthalmol* 2015; **160**(1): 62–71 e2.
34 Wei WB, Xu L, Jonas JB, Shao L, Du KF, Wang S *et al.* Subfoveal choroidal thickness: the Beijing Eye Study. *Ophthalmology* 2013; **120**(1): 175–180.
35 Nishida Y, Fujiwara T, Imamura Y, Lima LH, Kurosaka D, Spaide RF. Choroidal thickness and visual acuity in highly myopic eyes. *Retina* 2012; **32**(7): 1229–1236.
36 Ho M, Liu DT, Chan VC, Lam DS. Choroidal thickness measurement in myopic eyes by enhanced depth optical coherence tomography. *Ophthalmology* 2013; **120**(9): 1909–1914.
37 Zaben A, Zapata MA, Garcia-Arumi J. Retinal sensitivity and choroidal thickness in high myopia. *Retina* 2015; **35**(3): 398–406.
38 Moriyama M, Ohno-Matsui K, Futagami S, Yoshida T, Hayashi K, Shimada N *et al.* Morphology and long-term changes of choroidal vascular structure in highly myopic eyes with and without posterior staphyloma. *Ophthalmology* 2007; **114**(9): 1755–1762.
39 Quaranta M, Arnold J, Coscas G, Français C, Quentel G, Kuhn D *et al.* Indocyanine green angiographic features of pathologic myopia. *Am J Ophthalmol* 1996; **122**(5): 663–671.
40 Akyol N, Kukner AS, Ozdemir T, Esmerligil S. Choroidal and retinal blood flow changes in degenerative myopia. *Can J Ophthalmol* 1996; **31**(3): 113–119.
41 Read SA, Collins MJ, Vincent SJ, Alonso-Caneiro D. Choroidal thickness in myopic and nonmyopic children assessed with enhanced depth imaging optical coherence tomography. *Invest Ophthalmol Vis Sci* 2013; **54**(12): 7578–7586.
42 Ruiz-Moreno JM, Flores-Moreno I, Lugo F, Ruiz-Medrano J, Montero JA, Akiba M. Macular choroidal thickness in normal pediatric population measured by swept-source optical coherence tomography. *Invest Ophthalmol Vis Sci* 2013; **54**(1): 353–359.
43 Esmaeelpour M, Povazay B, Hermann B, Hofer B, Kajic V, Kapoor K *et al.* Three-dimensional 1060-nm OCT: choroidal thickness maps in normal subjects and improved posterior segment visualization in cataract patients. *Invest Ophthalmol Vis Sci* 2010; **51**(10): 5260–5266.
44 Wei YH, Yang CM, Chen MS, Shih YF, Ho TC. Peripapillary intrachoroidal cavitation in high myopia: reappraisal. *Eye (Lond)* 2009; **23**(1): 141–144.
45 Spaide RF, Akiba M, Ohno-Matsui K. Evaluation of peripapillary intrachoroidal cavitation with swept source and enhanced depth imaging optical coherence tomography. *Retina* 2012; **32**(6): 1037–1044.
46 Shimada N, Ohno-Matsui K, Yoshida T, Yasuzumi K, Kojima A, Kobayashi K *et al.* Characteristics of peripapillary detachment in pathologic myopia. *Arch Ophthalmol* 2006; **124**(1): 46–52.
47 Shimada N, Ohno-Matsui K, Nishimuta A, Tokoro T, Mochizuki M. Peripapillary changes detected by optical coherence tomography in eyes with high myopia. *Ophthalmology* 2007; **114**(11): 2070–2076.
48 Ohno-Matsui K, Akiba M, Moriyama M, Ishibashi T, Hirakata A, Tokoro T. Intrachoroidal cavitation in macular area of eyes with pathologic myopia. *Am J Ophthalmol* 2012; **154**(2): 382–393.

49 Curtin BJ. The posterior staphyloma of pathologic myopia. *Trans Am Ophthalmol Soc* 1977; **75**: 67–86.
50 Moriyama M, Ohno-Matsui K, Hayashi K, Shimada N, Yoshida T, Tokoro T *et al.* Topographic analyses of shape of eyes with pathologic myopia by high-resolution three-dimensional magnetic resonance imaging. *Ophthalmology* 2011; **118**(8): 1626–1637.
51 Henaine-Berra A, Zand-Hadas IM, Fromow-Guerra J, Garcia-Aguirre G. Prevalence of macular anatomic abnormalities in high myopia. *Ophthalmic Surg Lasers Imaging Retina* 2013; **44**(2): 140–144.
52 Chae JB, Moon BG, Yang SJ, Lee JY, Yoon YH, Kim JG. Macular gradient measurement in myopic posterior staphyloma using optical coherence tomography. *Korean J Ophthalmol* 2011; **25**(4): 243–247.
53 Rahimy E, Beardsley RM, Gomez J, Hung C, Sarraf D. Grading of posterior staphyloma with spectral-domain optical coherence tomography and correlation with macular disease. *Can J Ophthalmol* 2013; **48**(6): 539–545.
54 Park HY, Shin HY, Park CK. Imaging the posterior segment of the eye using swept-source optical coherence tomography in myopic glaucoma eyes: comparison with enhanced-depth imaging. *Am J Ophthalmol* 2014; **157**(3): 550–557.
55 Ohno-Matsui K, Akiba M, Modegi T, Tomita M, Ishibashi T, Tokoro T *et al.* Association between shape of sclera and myopic retinochoroidal lesions in patients with pathologic myopia. *Invest Ophthalmol Vis Sci* 2012; **53**(10): 6046–6061.
56 Fujiwara T, Imamura Y, Margolis R, Slakter JS, Spaide RF. Enhanced depth imaging optical coherence tomography of the choroid in highly myopic eyes. *Am J Ophthalmol* 2009; **148**(3): 445–450.
57 Curtin BJ, Teng CC. Scleral changes in pathological myopia. *Trans Am Acad Ophthalmol Otolaryngol* 1958; **62**(6): 777–788; discussion 88–90.
58 Shinohara K, Moriyama M, Shimada N, Nagaoka N, Ishibashi T, Tokoro T *et al.* Analyses of shape of eyes and structure of optic nerves in eyes with tilted disc syndrome by swept-source optical coherence tomography and three-dimensional magnetic resonance imaging. *Eye (Lond)* 2013; **27**(11): 1233–1241; quiz 42.
59 Ohno-Matsui K, Morishima N, Teramatsu T, Tokoro T, Nakagawa T. The long-term follow-up of a highly myopic patient with a macular vortex vein. *Acta Ophthalmol Scand* 1997; **75**(3): 329–332.
60 Ohno-Matsui K, Akiba M, Moriyama M, Shimada N, Ishibashi T, Tokoro T *et al.* Acquired optic nerve and peripapillary pits in pathologic myopia. *Ophthalmology* 2012; **119**(8): 1685–1692.
61 Gaucher D, Erginay A, Lecleire-Collet A, Haouchine B, Puech M, Cohen SY *et al.* Dome-shaped macula in eyes with myopic posterior staphyloma. *Am J Ophthalmol* 2008; **145**(5): 909–914.
62 Imamura Y, Iida T, Maruko I, Zweifel SA, Spaide RF. Enhanced depth imaging optical coherence tomography of the sclera in dome-shaped macula. *Am J Ophthalmol* 2011; **151**(2): 297–302.
63 Caillaux V, Gaucher D, Gualino V, Massin P, Tadayoni R, Gaudric A. Morphologic characterization of dome-shaped macula in myopic eyes with serous macular detachment. *Am J Ophthalmol* 2013; **156**(5): 958–67 e1.
64 Coco RM, Sanabria MR, Alegria J. Pathology associated with optical coherence tomography macular bending due to either dome-shaped macula or inferior staphyloma in myopic patients. *Ophthalmologica* 2012; **228**(1): 7–12.
65 Liang IC, Shimada N, Tanaka Y, Nagaoka N, Moriyama M, Yoshida T *et al.* Comparison of clinical features in highly myopic eyes with and without a dome-shaped macula. *Ophthalmology* 2015; **122**(8): 1591–1600.
66 Witmer MT, Margo CE, Drucker M. Tilted optic disks. *Surv Ophthalmol* 2010; **55**(5): 403–428.
67 Tay E, Seah SK, Chan SP, Lim AT, Chew SJ, Foster PJ *et al.* Optic disk ovality as an index of tilt and its relationship to myopia and perimetry. *Am J Ophthalmol* 2005; **139**(2): 247–252.
68 Kimura Y, Akagi T, Hangai M, Takayama K, Hasegawa T, Suda K *et al.* Lamina cribrosa defects and optic disc morphology in primary open angle glaucoma with high myopia. *PLoS One* 2014; **9**(12): e115313.
69 Cheung CY, Chen D, Wong TY, Tham YC, Wu R, Zheng Y *et al.* Determinants of quantitative optic nerve measurements using spectral domain optical coherence tomography in a population-based sample of non-glaucomatous subjects. *Invest Ophthalmol Vis Sci* 2011; **52**(13): 9629–9635.
70 Knight OJ, Girkin CA, Budenz DL, Durbin MK, Feuer WJ. Cirrus OCTNDSG. Effect of race, age, and axial length on optic nerve head parameters and retinal nerve fiber layer thickness measured by Cirrus HD-OCT. *Arch Ophthalmol* 2012; **130**(3): 312–318.
71 Wang Y, Xu L, Zhang L, Yang H, Ma Y, Jonas JB. Optic disc size in a population based study in northern China: the Beijing Eye Study. *Br J Ophthalmol* 2006; **90**(3): 353–356.
72 Qiu KL, Zhang MZ, Leung CK, Zhang RP, Lu XH, Wang G *et al.* Diagnostic classification of retinal nerve fiber layer measurement in myopic eyes: a comparison between time-domain and spectral-domain optical coherence tomography. *Am J Ophthalmol* 2011; **152**(4): 646–53 e2.
73 Kang SH, Hong SW, Im SK, Lee SH, Ahn MD. Effect of myopia on the thickness of the retinal nerve fiber layer measured by Cirrus HD optical coherence tomography. *Invest Ophthalmol Vis Sci* 2010; **51**(8): 4075–4083.
74 Kim NR, Lee ES, Seong GJ, Kang SY, Kim JH, Hong S *et al.* Comparing the ganglion cell complex and retinal nerve fibre layer measurements by Fourier domain OCT to detect glaucoma in high myopia. *Br J Ophthalmol* 2011; **95**(8): 1115–1121.
75 Shoji T, Nagaoka Y, Sato H, Chihara E. Impact of high myopia on the performance of SD-OCT parameters to detect glaucoma. *Graefes Arch Clin Exp Ophthalmol* 2012; **250**(12): 1843–1849.
76 Zhang C, Tatham AJ, Weinreb RN, Zangwill LM, Yang Z, Zhang JZ *et al.* Relationship between ganglion cell layer thickness and estimated retinal ganglion cell counts in the glaucomatous macula. *Ophthalmology* 2014; **121**(12): 2371–2379.
77 Panozzo G, Mercanti A. Optical coherence tomography findings in myopic traction maculopathy. *Arch Ophthalmol* 2004; **122**(10): 1455–1460.
78 Fujimoto M, Hangai M, Suda K, Yoshimura N. Features associated with foveal retinal detachment in myopic macular retinoschisis. *Am J Ophthalmol* 2010; **150**(6): 863–870.
79 Shimada N, Ohno-Matsui K, Yoshida T, Sugamoto Y, Tokoro T, Mochizuki M. Progression from macular retinoschisis to retinal detachment in highly myopic eyes

is associated with outer lamellar hole formation. *Br J Ophthalmol* 2008; **92**(6): 762–764.
80 Shimada N, Ohno-Matsui K, Nishimuta A, Moriyama M, Yoshida T, Tokoro T *et al.* Detection of paravascular lamellar holes and other paravascular abnormalities by optical coherence tomography in eyes with high myopia. *Ophthalmology* 2008; **115**(4): 708–717.
81 Shimada N, Tanaka Y, Tokoro T, Ohno-Matsui K. Natural course of myopic traction maculopathy and factors associated with progression or resolution. *Am J Ophthalmol* 2013; **156**(5): 948–57 e1.
82 Tanaka Y, Shimada N, Moriyama M, Hayashi K, Yoshida T, Tokoro T *et al.* Natural history of lamellar macular holes in highly myopic eyes. *Am J Ophthalmol* 2011; **152**(1): 96–99 e1.
83 Ellabban AA, Tsujikawa A, Matsumoto A, Yamashiro K, Oishi A, Ooto S *et al.* Three-dimensional tomographic features of dome-shaped macula by swept-source optical coherence tomography. *Am J Ophthalmol* 2013; **155**(2): 320–8 e2.
84 Hirakata A, Hida T. Vitrectomy for myopic posterior retinoschisis or foveal detachment. *Jpn J Ophthalmol* 2006; **50**(1): 53–61.
85 Shimada N, Sugamoto Y, Ogawa M, Takase H, Ohno-Matsui K. Fovea-sparing internal limiting membrane peeling for myopic traction maculopathy. *Am J Ophthalmol* 2012; **154**(4): 693–701.
86 Gomez-Resa M, Bures-Jelstrup A, Mateo C. Myopic traction maculopathy. *Dev Ophthalmol* 2014; **54**: 204–212.
87 Shimada N, Ohno-Matsui K, Yoshida T, Futagami S, Tokoro T, Mochizuki M. Development of macular hole and macular retinoschisis in eyes with myopic choroidal neovascularization. *Am J Ophthalmol* 2008; **145**(1): 155–161.
88 Chhablani J, Deepa MJ, Tyagi M, Narayanan R, Kozak I. Fluorescein angiography and optical coherence tomography in myopic choroidal neovascularization. *Eye (Lond)* 2015; **29**(4): 519–524.
89 Introini U, Casalino G, Querques G, Gimeno AT, Scotti F, Bandello F *et al.* in anti-VEGF treatment of myopic choroidal neovascularization. *Eye (Lond)* 2012; **26**(7): 976–982.
90 Leveziel N, Caillaux V, Bastuji-Garin S, Zmuda M, Souied EH. Angiographic and optical coherence tomography characteristics of recent myopic choroidal neovascularization. *Am J Ophthalmol* 2013; **155**(5): 913–919.
91 Battaglia Parodi M, Iacono P, Bandello F. Correspondence of leakage on fluorescein angiography and optical coherence tomography parameters in diagnosis and monitoring of myopic choroidal neovascularization treated with bevacizumab. *Retina* 2016; **36**(1): 104–109.
92 Khurana RN, Dupas B, Bressler NM. Agreement of time-domain and spectral-domain optical coherence tomography with fluorescein leakage from choroidal neovascularization. *Ophthalmology* 2010; **117**(7): 1376–1380.
93 Wong TY, Ohno-Matsui K, Leveziel N, Holz FG, Lai TY, Yu HG *et al.* Myopic choroidal neovascularisation: current concepts and update on clinical management. *Br J Ophthalmol* 2015; **99**(3): 289–296.
94 Spaide RF, Goldberg N, Freund KB. Redefining multifocal choroiditis and panuveitis and punctate inner choroidopathy through multimodal imaging. *Retina* 2013; **33**(7): 1315–1324.
95 Wolf S, Balciuniene VJ, Laganovska G, Menchini U, Ohno-Matsui K, Sharma T *et al.* RADIANCE: a randomized controlled study of ranibizumab in patients with choroidal neovascularization secondary to pathologic myopia. *Ophthalmology* 2014; **121**(3): 682–92 e2.
96 Ikuno Y, Ohno-Matsui K, Wong TY, Korobelnik JF, Vitti R, Li T *et al.* Intravitreal aflibercept injection in patients with myopic choroidal neovascularization: The MYRROR Study. *Ophthalmology* 2015; **122**(6): 1220–1227.
97 Yang HS, Kim JG, Kim JT, Joe SG. Prognostic factors of eyes with naive subfoveal myopic choroidal neovascularization after intravitreal bevacizumab. *Am J Ophthalmol* 2013; **156**(6): 1201–10 e2.
98 Bruyere E, Caillaux V, Cohen SY, Martiano D, Ores R, Puche N *et al.* Spectral-domain optical coherence tomography of subretinal hyperreflective exudation in myopic choroidal neovascularization. *Am J Ophthalmol* 2015; **160**: 749–758.e1.
99 Ohno-Matsui K, Kawasaki R, Jonas JB, Cheung CM, Saw SM, Verhoeven VJ *et al.* International photographic classification and grading system for myopic maculopathy. *Am J Ophthalmol* 2015; **159**(5): 877–83 e7.
100 Spaide RF. Age-related choroidal atrophy. *Am J Ophthalmol* 2009; **147**(5): 801–810.
101 Wang NK, Lai CC, Chou CL, Chen YP, Chuang LH, Chao AN *et al.* Choroidal thickness and biometric markers for the screening of lacquer cracks in patients with high myopia. *PLoS One* 2013; **8**(1): e53660.
102 Hayashi K, Ohno-Matsui K, Shimada N, Moriyama M, Kojima A, Hayashi W *et al.* Long-term pattern of progression of myopic maculopathy: a natural history study. *Ophthalmology* 2010; **117**(8): 1595–1611, 611 e1-4.
103 Tanaka Y, Shimada N, Ohno-Matsui K. Extreme thinning or loss of inner neural retina along the staphyloma edge in eyes with pathologic myopia. *Am J Ophthalmol* 2015; **159**(4): 677–682.
104 Kolb JP, Klein T, Kufner CL, Wieser W, Neubauer AS, Huber R. Ultra-widefield retinal MHz-OCT imaging with up to 100 degrees viewing angle. *Biomed Opt Express* 2015; **6**(5): 1534–1552.
105 Forte R, Cennamo G, Pascotto F. de Crecchio G. En face optical coherence tomography of the posterior pole in high myopia. *Am J Ophthalmol* 2008; **145**(2): 281–288.
106 Tao A, Shao Y, Zhong J, Jiang H, Shen M, Wang J. Versatile optical coherence tomography for imaging the human eye. *Biomedical optics express* 2013; **4**(7): 1031–1044.
107 Yu J, Jiang C, Wang X, Zhu L, Gu R, Xu H *et al.* Macular perfusion in healthy chinese: an optical coherence tomography angiogram study. *Invest Ophthalmol Vis Sci* 2015; **56**(5): 3212–3217.